

Ordering Process and Age-hardening Mechanism of CuPd-AuCu Pseudo-binary Alloys

Takanobu SHIRAISHI, Michio OHTA and Masaji YAMANE

Department of Dental Materials Engineering, Faculty of Dentistry, Kyushu University, Maidashi, Higashi-ku, Fukuoka 812, Japan

Received on September 7, 1984

Ordering process and age-hardening mechanism of CuPd-AuCu pseudo-binary alloys were examined. In alloys with electron-atom ratios (e/a) < 0.87, short range ordering was observed in the early stage of aging, thereafter, long range ordering occurred from grain boundaries by heterogeneous ordering mechanism. Age-hardening of these alloys was attained by the increase in volume fractions of CuPd and/or AuCuI phases. On the other hand, in alloys with e/a > 0.87, fine domains of AuCuI type superlattice were formed very rapidly in the grain interior. The elastic strain field generated by this reaction caused age-hardening.

Key Words: Au-Pd-Cu alloys, Age-hardening, Electron microscopy

I. INTRODUCTION

Several studies on the age-hardening mechanisms of dental precious metal alloys have been carried out on commercial alloys and primary ternary alloys such as the Au-Cu-Ag, Ag-Pd-Cu and Au-Pd-Cu systems. Results of those studies revealed that ordering and phase separation played a very important role in age-hardening. Especially, formation of AuCu and CuPd superlattices was found to contribute greatly to the age-hardening of the dental precious metal alloys.

Much attention should be paid to Au-Pd-Cu ternary system, because both AuCu and CuPd superlattices are formed in this system. A few studies have been performed on the age-hardening behavior of Au-Pd-Cu ternary alloys. Kumazawa et al.^{1,2)} studied the ordering process and mechanical properties of CuPd-Au pseudo-binary alloys. Ordering rate of the CuPd phase was found to decrease with the increase in gold content. Metahi³⁾ studied the age-hardening process of AuCu-Pd pseudo-binary alloys. His study revealed that a maximum hardness was attained in a AuCu-12.0at%Pd alloy and that the ordering process of alloys containing less than 12.0at%Pd was analogous to that of an equiatomic AuCu alloy.

Nevertheless, the ordering processes and age-hardening mechanisms of alloys whose compositions are in (CuPd+AuCu) two phase coexistent region and in AuCu single phase region containing a great deal of palladium have not yet been elucidated.

According to the phase diagram of Au-Pd-Cu ternary system³⁾, (CuPd+AuCu) two phase coexistent region exists in the central part of CuPd-AuCu pseudo-binary system, and ordering region of AuCu widely spreads toward CuPd (Cu-40at%Pd). Consequently, the problems described above can be solved by studying the ordering process and the age-hardening behavior of the alloys in the CuPd-AuCu pseudo-binary system.

In this work, ordering process and age-hardening behavior of several alloys in the CuPd-AuCu pseudo-binary system were investigated by means of electrical resistivity measurement, X-ray diffraction, transmission electron microscopy and hardness test. The ordering process and the age-hardening mechanism of alloys whose compositions were in (CuPd+AuCu) two phase coexistent region and of AuCu single phase alloy with high palladium content were examined.

II. MATERIALS AND METHODS

Au-Pd-Cu ternary alloys whose compositions were in the CuPd-AuCu pseudo-binary system were prepared by melting 99.99% Au, Pd and Cu in vacuo. By alternate swaging and annealing of the ingots, wires of 1.0 mm in diameter were prepared. Chemical compositions of alloys are listed in Table 1. The CuPd-AuCu pseudo-binary phase diagram⁴⁾ is illustrated in Fig. 1 together with symbols of alloys. At lower temperatures, compositions of alloys A and B exist in CuPd single phase region, those of alloys F and G in AuCu single phase region, while those of alloys C, D and E in (CuPd+AuCu) two phase coexistent region.

Specimens were solution treated at 973K for 1.8 ks in high purity argon gas stream and quenched into ice brine. After this solution treatment, specimens were aged at 573K for various periods in a salt bath and quenched into ice brine. Electrical resistivity of the specimen was measured at liquid nitrogen temperature by using the four-terminal potentiometric method with a direct current of 500 mA.

Powder specimens (fine enough to pass through 200 mesh sieve) were prepared by filing the wire using a diamond disk. They were sealed in an evacuated silica tube and subjected to the heat treatment. X-ray diffraction was performed by a diffractometer

Table 1 Chemical compositions of alloys.

Alloy		Cu	Pd	Au
A	at% (mass%)	57.69 (44.88)	42.31 (55.12)	0 (0)
B	at% (mass%)	58.37 (42.44)	34.99 (42.60)	6.64 (14.96)
C	at% (mass%)	57.31 (39.37)	30.93 (35.58)	11.76 (25.05)
D	at% (mass%)	56.93 (38.03)	28.59 (31.98)	14.48 (29.99)
E	at% (mass%)	55.59 (35.89)	26.92 (29.10)	17.49 (35.01)
F	at% (mass%)	54.80 (33.32)	21.34 (21.72)	23.86 (44.96)
G	at% (mass%)	49.4 (24.0)	0 (0)	50.6 (76.0)

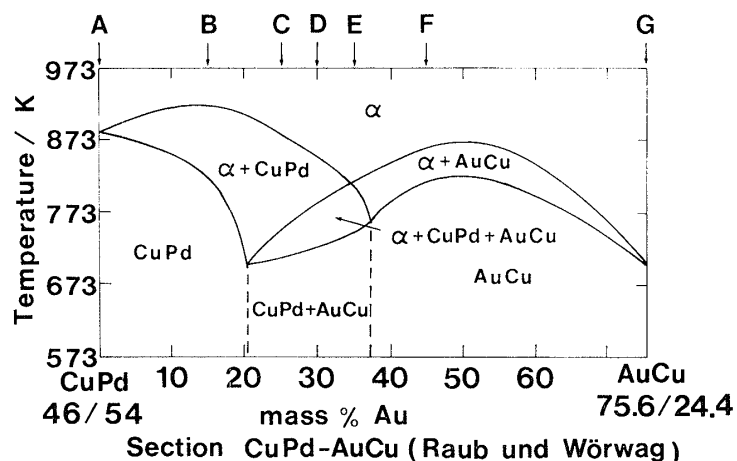


Figure 1 Phase diagram of the CuPd-AuCu pseudo-binary system.

(RU-100PL), using Ni filtered $\text{CuK}\alpha$ radiation at 45 kV and 80 mA.

Disks of three mm in diameter were punched out of the heat treated sheet specimens. They were electrolytically thinned by the jet polishing technique. The electrolyte used was a solution of 35 g of CrO_3 , 200 cm^3 of CH_3COOH and 10 cm^3 of H_2O . The transmission electron microscope used was a JEM-1000 (HVEM Lab., Kyushu University) operating at 1 MV.

Hardness test was carried out on the appropriately heat treated specimens with a load of 2.94 N using a micro-Vickers hardness tester. The average hardness value was obtained from five indentations.

III. EXPERIMENTAL RESULTS

1. Ordering Rate

Figures 2 (a) and 2 (b) show change in electrical resistivity of alloys A~G aged at

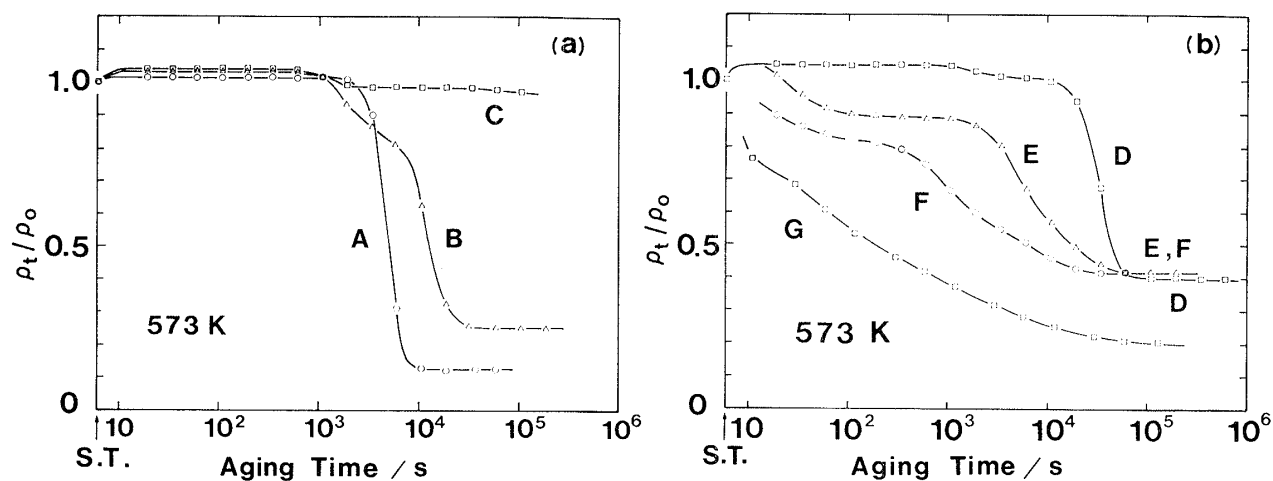


Figure 2 Change in electrical resistivity of alloys A, B, C (a) and D, E, F, G (b) aged at 573K. Symbols ρ_0 and ρ_t represent electrical resistivity of the alloy as solution treated and at the aging time of t seconds, respectively.

573K. The falling rate of resistivity of alloy B containing 6.64at% Au was lower than that of alloy A. Hence, gold addition decrease the ordering rate of CuPd, as demonstrated by Kumazawa¹⁾. On the other hand, the time at which resistivity began to decrease shifted toward longer aging time side with Pd content in AuCu, as shown in Fig. 2 (b). This suggests that Pd addition decreases the ordering rate of AuCu.

2. Short Range Ordering

As shown in Figs. 2 (a) and 2 (b), electrical resistivity slightly increased in the early stage of aging in alloys A~D. This increase is thought to be due to the short range ordering in α phase⁵⁾.

Figure 3 is an electron diffraction pattern taken from α phase of alloy D aged at 573K for 180 s. By this heat treatment, electrical resistivity increased as much as 4.6%. The incident electron beam is parallel to $[00\bar{1}]_{\alpha}$. Fourfold and twofold splittings of the diffuse scattering are visible at 110, 100 and their equivalent positions, respectively. These diffuse scatterings were interpreted to be due to the short range ordering in α phase⁶⁾. Accordingly, it was revealed that a slight increase in electrical resistivity observed in the early stage of aging in alloys A~D originated from the short range ordering.

Figure 4 is a time temperature transformation diagram of alloy F confirmed by transmission electron microscopy. The symbol \times denotes the short range ordering in α phase. It is obvious that the short range ordering proceeds over a wide range of temperatures in the early stage of aging in this alloy. The short range ordering is not considered to proceed in AuCu single phase alloys containing less than 12.0at% Pd³⁾. Therefore, ordering process of alloy F containing 21.34at% Pd was found to be quite different from that of AuCu single phase alloys which contained low concentrations of palladium.

It has been clarified that the short range ordering occurred in the early stage of aging

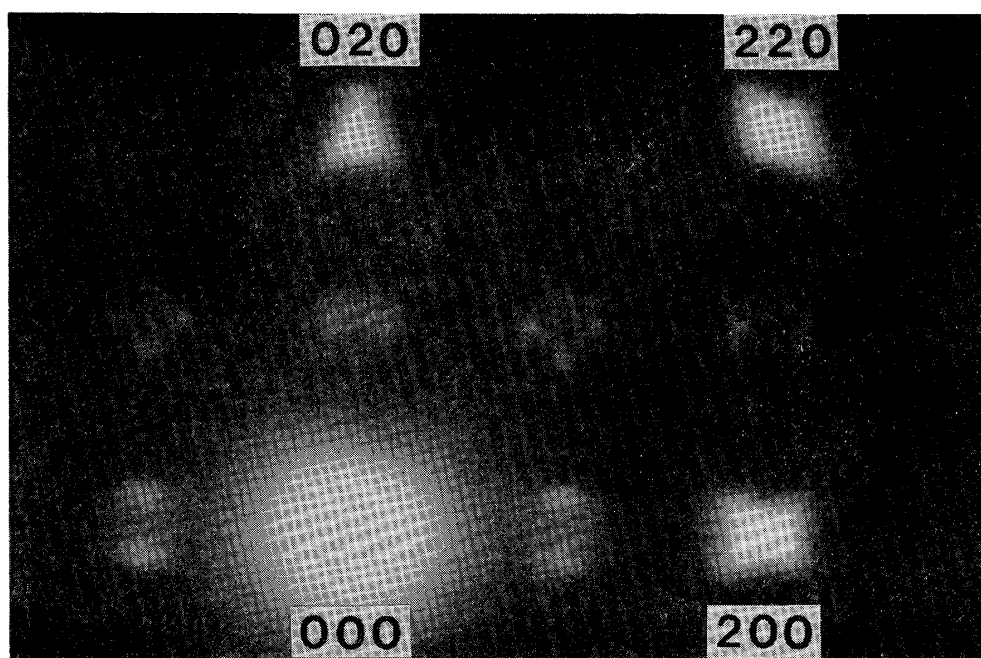


Figure 3 Electron diffraction pattern of alloy D aged at 573K for 180s.

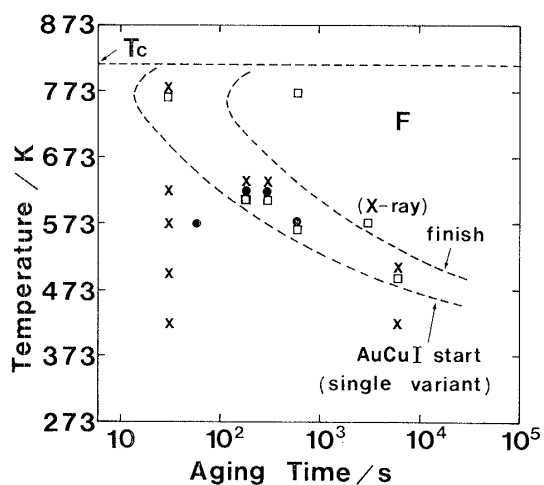


Figure 4 Time temperature transformation diagram of alloy F. The symbol \times denotes short range ordering in the grain interior. Symbols \bullet and \square denote the formation of long range order in the grain interior and at the grain boundary, respectively.

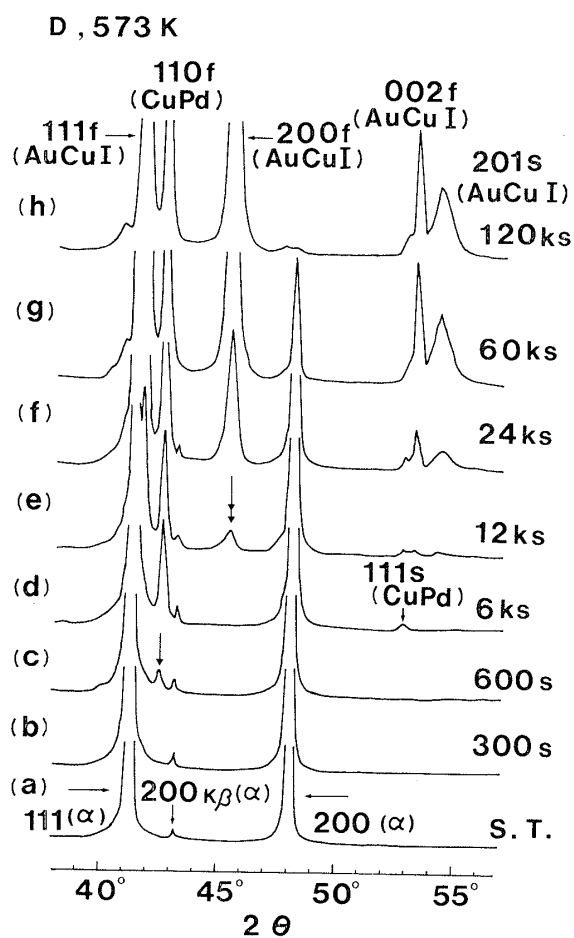


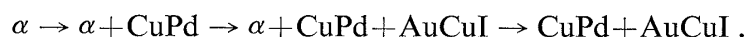
Figure 5 Change in X-ray diffraction pattern of alloy D aged at 573K

in all the alloys examined in this work, except for the equiatomic AuCu binary alloy.

3. Long Range Ordering

(1) X-ray diffraction

Figure 5 shows change in X-ray diffraction pattern of alloy D aged at 573K. A weak 110 fundamental line of the ordered CuPd phase (\downarrow) and the 200 fundamental line of the ordered AuCuI phase (\downarrow) appeared at the aging time of 600 s and 12 ks, respectively. Their intensity increased with aging time. However, the intensity of α phase peaks gradually decreased and completely disappeared at 120 ks. On the other hand, diffraction angles of each phase were unchanged during the ordering reaction. Therefore, it can be concluded that the ordering in alloy D proceeds by the heterogeneous ordering mechanism. As seen in Fig. 5, the ordered CuPd phase was formed prior to the ordered AuCuI phase. The ordering process of alloy D is, accordingly, described as follows:



Change in X-ray diffraction pattern of alloy F suggested that the ordering behavior of alloy F was the same as that of alloy D, except that the equilibrium phase at 573K is AuCuI single phase.

(2) Transmission electron microscopy

Figure 6 (a) is a bright-field image of alloy D aged at 573K for 180 ks, showing a fully ordered structure. Grain boundaries are clearly seen, but no contrast is visible in the grain interior except for thickness extinction contours. Figure 6 (b) shows a selected area diffraction pattern taken from the region in the circle of Fig. 6 (a). This diffraction pattern corresponds to a 001 reciprocal lattice plane of a single variant AuCuI phase. Therefore, the ordered AuCuI phase was found to exist as coarse grains in equilibrium state.

Figure 7 (a) is an electron diffraction pattern taken from alloy F aged at 573K for 60 s. Incident beam was parallel to $[00\bar{1}]_a$. Fundamental and weak superlattice spots of AuCuI type superlattice, which are arranged in three variants, are visible as well as normal spots of α phase. Figure 7 (b) is a dark-field image taken by using 001 superlattice spot. Fine domains of AuCuI type superlattice can be seen to be oriented in two direc-

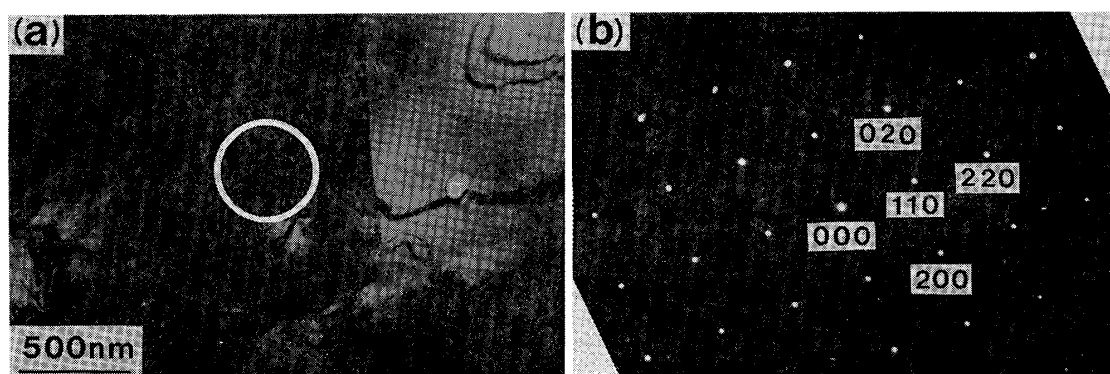


Figure 6 Bright-field image (a) and selected area diffraction pattern taken from the region in the circle (b) of alloy D aged at 573K for 180ks.

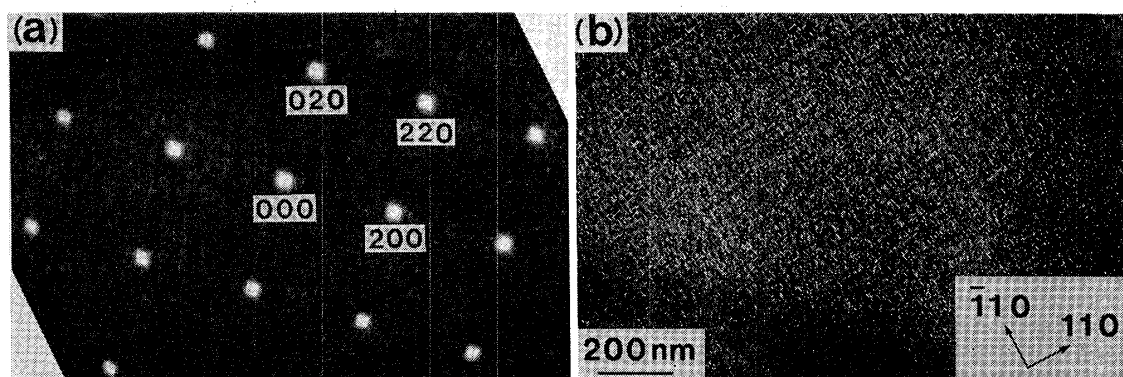


Figure 7 Electron diffraction pattern of alloy F aged at 573K for 60s (a) and dark-field image taken by using 001 superlattice spot (b).

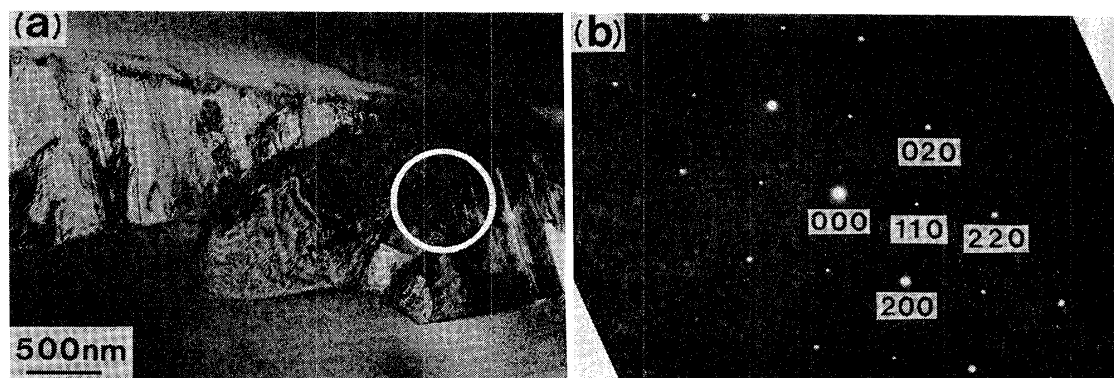


Figure 8 Bright-field image (a) and selected area diffraction pattern taken from the region in the circle (b) of alloy F aged at 573K for 600s.

tions, i.e., $[110]$ and $[\bar{1}10]$ directions. These observations lead to the conclusion that fine domains of AuCuI type superlattice are formed in the grain interior and that their a - and c -axes are parallel to cube edge directions of matrix fcc. Formation of fine AuCuI ordered domains was also observed at 623K, as shown in Fig. 4 (●).

Figure 8 (a) is a bright-field image of alloy F aged at 573K for 600 s, showing a newly produced phase at the grain boundary. Figure 8 (b) shows a selected area diffraction pattern taken from the region in the circle of Fig. 8 (a). These image and pattern are analogous to those of alloy D shown in Figs. 6 (a) and 6 (b). Consequently, it is concluded that the long range ordering in alloy F is also attained by the heterogeneous ordering mechanism.

4. Age-hardening Behavior

Figure 9 shows age-hardening curves of alloys D~G aged at 573K. Hardness of alloy D did not vary up to the aging time of 600 s, but it gradually increased thereafter and was followed by a marked increase to attain its maximum value in 120 ks.

Age-hardening of alloy F occurred simultaneously with aging. Hardness of this alloy attained its maximum value in 600 s and was followed by the constant value. Hardness of alloy G (equiatomic AuCu alloy) increased very rapidly to attain its maximum value in 60 s, then decreased gradually.

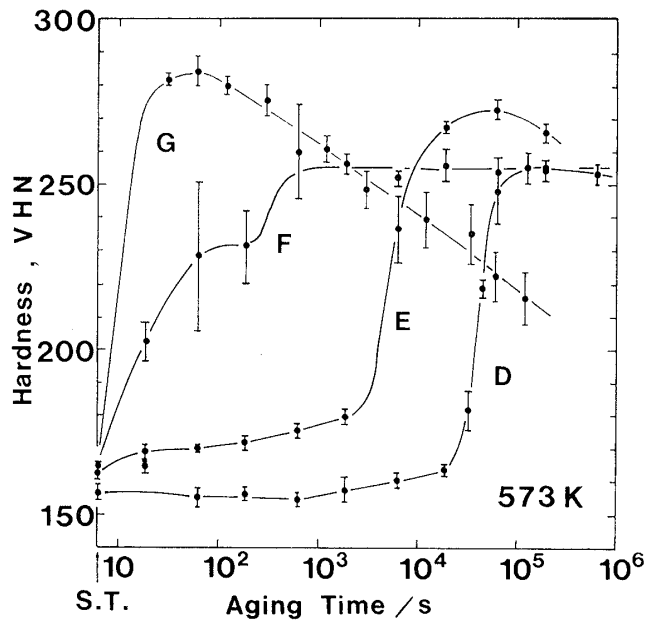


Figure 9 Age-hardening curves of alloys D, E, F and G aged at 573K.

IV. DISCUSSION

1. Relation between Ordering Process and Electron-Atom Ratio

Figure 10 represents a schematic illustration of the electron diffraction pattern shown in Fig. 3. As already mentioned, this electron diffraction pattern was obtained from the short range ordered α phase. The separation m of intensity maxima of diffuse scatterings at 110 position was measured in terms of the distance between 000 and 200 spots for alloys A, D and F. Figure 11 shows relation between m value and electron-atom ratio, e/a .

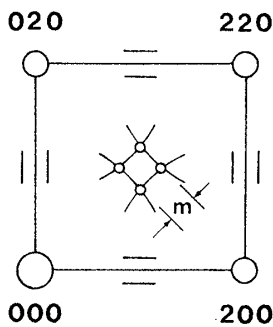


Figure 10 Schematic illustration of diffuse scatterings in Figure 3.

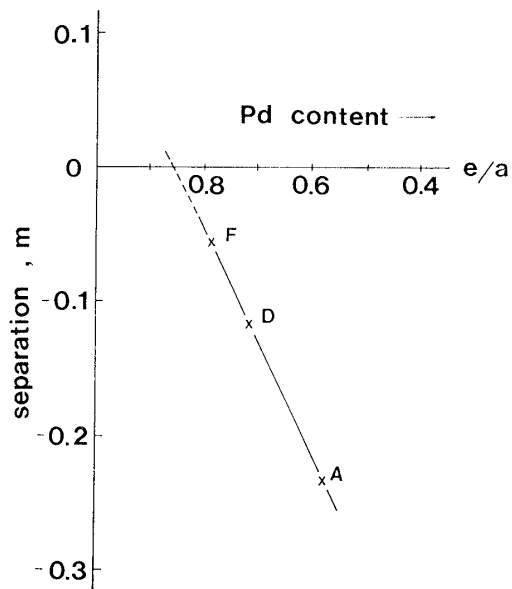


Figure 11 Measured values of separation m vs. electron-atom ratio, e/a .

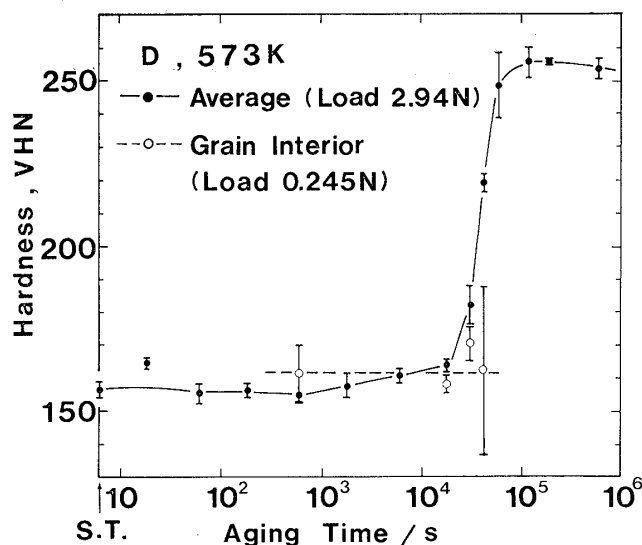


Figure 13 Age-hardening curve of alloy D aged at 573K.

investigate the age-hardening mechanism of alloy D, change in hardness in the grain interior was examined. As shown in Fig. 13, hardness in the grain interior did not vary, while the average hardness markedly increased after the aging time of about 18 ks. This finding means that hardening does not occur in the grain interior and that age-hardening of alloy D is due to the increase in volume fractions of ordered CuPd and AuCuI phases. Comparing X-ray diffraction pattern with age-hardening curve, it is apparent that the formation of AuCuI phase corresponds to the marked increase in hardness. Consequently, the AuCuI phase is considered to play a more significant role in the age-hardening than the CuPd phase.

Age-hardening of alloy F occurs simultaneously with aging at 573K. As previously described, fine domains of AuCuI type superlattice were formed in the grain interior in the early stage of aging. Both diffraction pattern and dark-field image obtained from the grain interior of age-hardened alloy F (Figs. 7 (a) and 7 (b)) resemble very closely those of age-hardened equiatomic AuCu alloy in feature. Therefore, age-hardening mechanism of alloy F in the early stage of aging at 573K is considered to be the same as that of equiatomic AuCu alloy. That is to say, elastic strain field generated by the formation of fine domains of AuCuI type superlattice that are coherent with the matrix leads to the age-hardening of alloy F. But the age-hardening mechanism changes at the aging time of about 1 ks into that of alloy D, indicating that hardening is due to the increase in volume fraction of grain boundary products (large size AuCuI).

Formation of AuCuI type superlattice in the grain interior of alloy F was also observed at the aging temperature of 623K. However this reaction is unstable. Figure 14 shows the reproducibility of age-hardening curve of alloy F aged at 573K. The scatter of the hardness values was very large up to attaining the maximum hardness value. Moreover, this feature was found to be well reproducible. The age-hardening of alloy F aged at 573K originated from the elastic strain field in the grain interior generated by the formation of fine domains of AuCuI type superlattice. Therefore, the large scatter of hard-

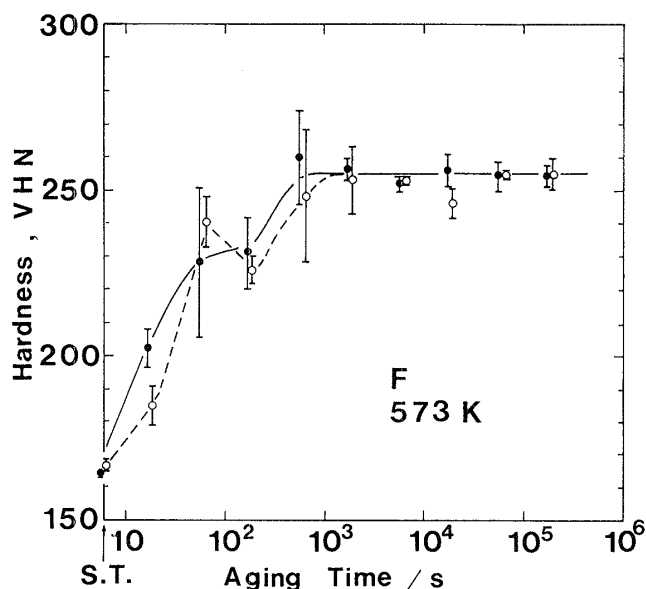


Figure 14 Reproducibility of age-hardening curve of alloy F aged at 573K.

ness values observed in the age-hardening process implies that the magnitude of development of AuCuI type superlattice markedly varies with the position of the specimen. In fact, transmission electron microscopy confirmed the validity of this interpretation. Consequently, formation of AuCuI type superlattice in the grain interior of alloy F is unstable.

V. CONCLUSION

Ordering process and age-hardening behavior of several alloys in the CuPd-AuCu pseudo-binary system were investigated by means of electrical resistivity measurement, X-ray diffraction, transmission electron microscopy and hardness test.

Ordering process of alloys in the CuPd-AuCu pseudo-binary system strongly depended on electron-atom ratio, e/a . In the alloys with $e/a < 0.87$, short range ordering proceeded in the early stage of aging. In these alloys, long range ordering occurred from the grain boundaries by the heterogeneous ordering mechanism. On the other hand, in the alloys with $e/a > 0.87$, fine domains of long range ordered AuCuI type superlattice were formed very rapidly in the grain interior.

In the alloys with $e/a < 0.87$, age-hardening was attained by the increase in volume fractions of long range ordered phases such as CuPd and/or AuCuI which were formed at the grain boundaries. On the other hand, in the alloys with $e/a > 0.87$, age-hardening was attributed to the elastic strain field in the grain interior generated by the formation of fine domains of AuCuI type superlattice. But in alloy F ($e/a = 0.787$), fine domains of AuCuI type superlattice were exceptionally formed in the grain interior when the alloy was aged at 573K or 623K. This reaction contributed to the age-hardening.

REFERENCES

- 1) Kumazawa, T.: Studies on the dental gold-alloys (9), *J. Japan Soc. Dent. Appar. Mater.*, **8**: 197-

- 204, 1967, (in Japanese).
- 2) Kumazawa, T., Yasuda, K., Metahi, H. and Kanzawa, Y.: Studies on the dental gold-alloys (12), *J. Japan Soc. Dent. Appar. Mater.*, **13**: 230-236, 1972, (in Japanese).
 - 3) Metahi, H.: Studies on the dental gold-alloys (15), *J. Japan Soc. Dent. Appar. Mater.*, **17**: 120-131, 1976, (in Japanese).
 - 4) Raub, E. und Wörwag, G.: Über Gold-Palladium-Kupfer-Legierungen, *Z. Metallkde.*, **46**: 119-128, 1955.
 - 5) Shiraishi, T.: Ordering process in CuPd alloys during continuous heating, *J. Japan Inst. Metals*, **46**: 245-252, 1982, (in Japanese).
 - 6) Ohshima, K. and Watanabe, D.: Electron diffraction study of short-range-order diffuse scattering from disordered Cu-Pd and Cu-Pt alloys, *Acta Cryst.*, **A29**: 520-526, 1973.

値が赤外炉焼成物において高値を示し、他の測定値はすべて赤外炉焼成物が低値を示した。また COLOR TABLE と各陶材焼成物とは色彩において両者の相違が見

られ、白金炉と赤外炉などの熱源によっても陶材焼成物に色調の変化が表われた。

サイクリック・クリープのコンピュータシミュレーション

和田正高, 菅原敏, 埴隆夫, 大川昭治, 近藤清一郎, 太田 守

北海道大学歯学部歯科理工学教室

臨床で認められているように、義歯床の破折の大きな原因の一つは疲労である。これを究明するために、著者らはサイクリック・クリープ・テストを設計製作し、その試用結果を先に報告した。

さらに本研究では、サイクリック・クリープの数値解析として、FEM をコアとするシミュレータを開発し、パーソナルコンピュータを使用してシミュレーションを行った。

試験方法として、JIS 及び ADAS に基づく片振り曲げ負荷を採用した。材料はエンジニアリングプラスチックの内から PEEK を採りあげた。この材料の DENTURE 使用時を想定してシミュレーションを行い、二、三の興味ある結果を得たので報告する。

なお、本研究は歯科領域における CAE としての試みであるが、なお機器の面で増強の予定がある。

各種歯科用アマルガムアロイの特性と、 練和時間がその物理的諸性質に及ぼす影響

中井宏之, 鈴木一臣, 入江正郎, 長山克也*, 橋本弘一*

岡山大学歯学部歯科理工学講座

*城西歯科大学歯科材料学講座

入手可能な低、高銅型アマルガムアロイの物理的諸性質を主として A. D. A. 規格 No. 1 の方法によって測定してその特性を比較、考察した。同時に、練和時間の変化がこれらの物理的諸性質に及ぼす影響についても検討した。

低銅型アロイにおいては粒状が物理的諸性質に及ぼす影響は比較的小さかったが、高銅型アロイでは著明であった。即ち、球状粒子のみで構成されている単一組成型高銅アロイは他のすべてのアロイに比べて際立った特徴を示した。即ち、低銅型アロイは勿論、配合型高銅ア

ロイも明らかに異なった特徴を持つことがわかった。

練和時間が物理的諸性質に及ぼす影響についてみると、不十分な練和は低、高銅型を問わず削片状アロイの性質に著しい悪影響を及ぼすが、球状アロイにはその影響が比較的小さいことがわかった。製造者の指示よりも過剰に練和した場合は機械的性質は若干向上するが、著しい発熱、操作時間の短縮、硬化時の収縮を伴うので臨床的に利点があるとは思われなかった。物理的諸性質のうちで練和時間の影響を特に著明に表わしたのは、クリープであった。

CuPd-AuCu 擬 2 元合金の規則化過程と時効硬化機構

白石孝信, 太田道雄, 山根正次

九州大学歯学部歯科理工学教室

CuPd-AuCu 擬 2 元合金の規則化と時効硬化機構を検討した。e/a 値 (伝導電子濃度) が 0.87 より小さい合金では時効初期に短範囲規則化が進行し、その後不均一規

則化機構により長範囲規則化が結晶粒界から起こった。これらの合金の時効硬化は CuPd 相または AuCu I 相の体積率の増加によるものであった。一方、e/a 値が

0.87より大きい合金では AuCu I 型規則格子の微細なドメインが粒内に速やかに形成された。この反応により引き起こされる弾性ひずみ場が時効硬化の原因であった。

タンニン・フッ化物合剤 (HY 剤) の配合された 合着用セメントの長期浸水による物性の変化

入江正郎, 鈴木一臣, 中井宏之

岡山大学歯学部歯科理工学講座

タンニン・フッ化物合剤 (HY 剤) の配合されたカルボキシレートセメントとリン酸セメントについて長期間の浸水に伴う物理的性質の変化を検討し、フッ化物の配合されていない同種セメントと比較した。

圧縮、引張り強さについてみると、カルボキシレートセメントの場合には HY 剤配合による影響などはほとんどみられないが、リン酸セメントの場合には、強さが明らか

かに増加した。寸法変化、吸水性についてみると、HY 剤の配合されたカルボキシレートセメントの場合、12ヶ月の浸水後では配合されていないものの約2倍の収縮を示し、吸水率も硬化後の早期からわずかながら増加した。一方、リン酸セメントの場合にも、HY 剤を配合されたものの方が収縮も吸水率も逆にわずかながら減少した。

有機酸中におけるガラスイオノマーセメントの侵食過程

松家茂樹, 松家洋子*, 山本 泰*, 山根正次

九州大学歯学部歯科理工学講座

*九州大学歯学部歯科保存学第二講座

酢酸、乳酸、クエン酸および塩酸中におけるガラスイオノマーセメントの侵食過程を化学分析、SEM 観察および赤外吸光分析により検討した。

各酸の陰イオンと Al 又は Ca との錯体の安定度定数が大きい程あるいは、酸溶液の pH が低い程、Al, Ca, Na, Si および F の溶出量が多くなった。SEM 観

察により、0.01 M クエン酸および塩酸中ではセメントマトリックスが溶解することが分かった。0.01 M クエン酸および塩酸中では、セメント浸漬後に白色沈殿が生成した。その沈殿は、水和ケイ酸質ゲルであることが IR スペクトルによりわかった。

人エナメル質に対する酸処理法の効果 (酸処理法の臨床応用の改善)

武 谷 道 彦

九州大学歯学部歯科保存第二講座

エナメル質酸処理法に関する研究として、エナメル質の酸処理面や接着破壊面を SEM を用いて観察した。また、酸処理に伴う Ca の溶出量、中心線平均アラサ、接着強さの測定を行った。その結果、まず小柱中心部が窪み、次に小柱辺縁に狭い溝が形成され、酸処理時間が長くなる程溝は広く深くなった。接着破壊面には、レジンとエナメル質の破折が観察された。リン酸はすべての測定値において大きな値を示した。シトラコン酸とピルビ

ン酸は、Ca の溶出量はリン酸の約半分であったが、それ以外の測定値はリン酸とほぼ等しかった。クエン酸はすべての測定値で最小の値を示した。Ca の溶出量と接着強さは、酸の濃度が増加するにしたがい一定の値までは増加するが、その後減少した。すべての測定値は、酸処理時間が長くなる程増加した。シトラコン酸の臨床使用の可能性が示唆された。